

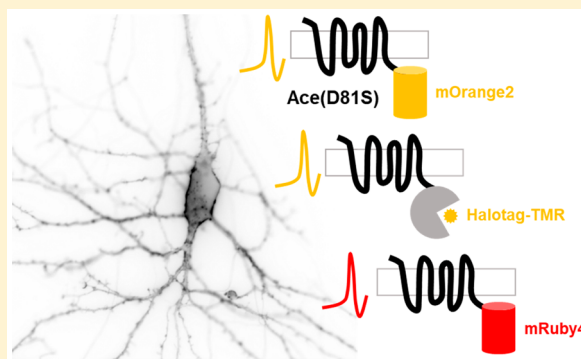
## Imaging Neuronal Activity with Fast and Sensitive Red-Shifted Electrochromic FRET Indicators

Yongxian Xu,<sup>†,‡,§</sup> Mengying Deng,<sup>||,#</sup> Shu Zhang,<sup>||,#</sup> Junqi Yang,<sup>⊥</sup> Luxin Peng,<sup>‡</sup> Jun Chu,<sup>\*,||</sup> and Peng Zou<sup>\*,‡,§,Ⓜ</sup><sup>†</sup>School of Life Sciences, Tsinghua University, Beijing 100084, China<sup>‡</sup>College of Chemistry and Molecular Engineering, Synthetic and Functional Biomolecules Center, Beijing National Laboratory for Molecular Sciences, Key Laboratory of Bioorganic Chemistry and Molecular Engineering of Ministry of Education, Peking University, PKU-IDG/McGovern Institute for Brain Research, Beijing 100871, China<sup>§</sup>Peking-Tsinghua Center for Life Sciences, Beijing, China<sup>||</sup>Laboratory for Biomedical Optics and Molecular Imaging, CAS Key Laboratory of Health Informatics, Shenzhen Institute of Synthetic Biology, Shenzhen-Hong Kong Institute of Brain Science, Shenzhen Institutes of Advanced Technology, Chinese Academy of Sciences, Shenzhen 518055, China<sup>⊥</sup>Peking-Tsinghua-NIBS Joint Graduate Program, Peking University, Beijing 100871, China

## Supporting Information

**ABSTRACT:** Genetically encoded voltage indicators (GEVIs) allow optical recording of neuronal activities with high spatial resolution. While most existing GEVIs emit in the green range, red-shifted GEVIs are highly sought after because they would enable simultaneous stimulation and recording of neuronal activities when paired with optogenetic actuators, or two-color imaging of signaling and neuronal activities when used along with GFP-based indicators. In this study, we present several improved red-shifted GEVIs based on the electrochromic Förster resonance energy transfer (eFRET) between orange/red fluorescent proteins/dyes and rhodopsin mutants. Through structure-guided mutagenesis and cell-based sensitivity screening, we identified a mutant rhodopsin with a single mutation that exhibited more than 2-fold improvement in voltage sensitivity. Notably, this mutation has been independently discovered by Pieribone et al. (Pieribone, V. A. et al. *Nat Methods* 2018, 15 (12), 1108–1116). In cultured rat hippocampal neurons, our sensors faithfully reported action potential waveforms and subthreshold activities. We also demonstrated that this mutation could enhance the sensitivity of hybrid indicators, thus providing insights for future development.

**KEYWORDS:** Voltage imaging, fluorescent proteins, rhodopsin, optogenetics



Membrane potential is a fundamental biophysical signal that underlies neuronal activity. Over the past decades, electrode-based recording of membrane potential has greatly advanced our understanding of neuronal signaling dynamics at millisecond time scales. The patch clamp technique, while powerful, is often limited by low throughput and invasiveness to cells, and it does not easily resolve the subcellular distribution of membrane potential. Optical recording of membrane potential with fluorescent voltage indicators, including synthetic dyes,<sup>1</sup> genetically encoded sensors,<sup>2</sup> and hybrid indicators,<sup>3</sup> could complement electrode-based methods by offering high spatial resolution, minimal invasiveness, and highly parallel measurement.

Development of genetically encoded voltage indicators (GEVIs) in recent years has mainly capitalized on two distinct voltage-sensing mechanisms. The first approach utilizes voltage-dependent conformational changes in the voltage-

sensing domain (VSD) of a voltage-sensing phosphatase from *Ciona intestinalis*<sup>4–6</sup> or *Gallus gallus*.<sup>7</sup> When a fluorescent protein (FP) or an FP pair is fused to a VSD, its fluorescence emission can become sensitive to the membrane potential. With this strategy, VSFP series and ArcLight series were developed and reported action potentials (APs) and subthreshold activities in cultured neurons, brain slices, and in vivo.<sup>5,8</sup> By inserting a circularly permuted GFP (cpGFP) into an extracellular loop of a VSD, the ASAP series exhibited fast response to membrane voltage and enabled high-speed tracking of APs in vivo.<sup>7,9,10</sup> More recently, a red-shifted GEVI was developed by fusing cpmApple to the C-terminus of VSD to achieve voltage imaging in brain slices.<sup>6</sup>

Received: September 12, 2019

Accepted: November 14, 2019

Published: November 14, 2019

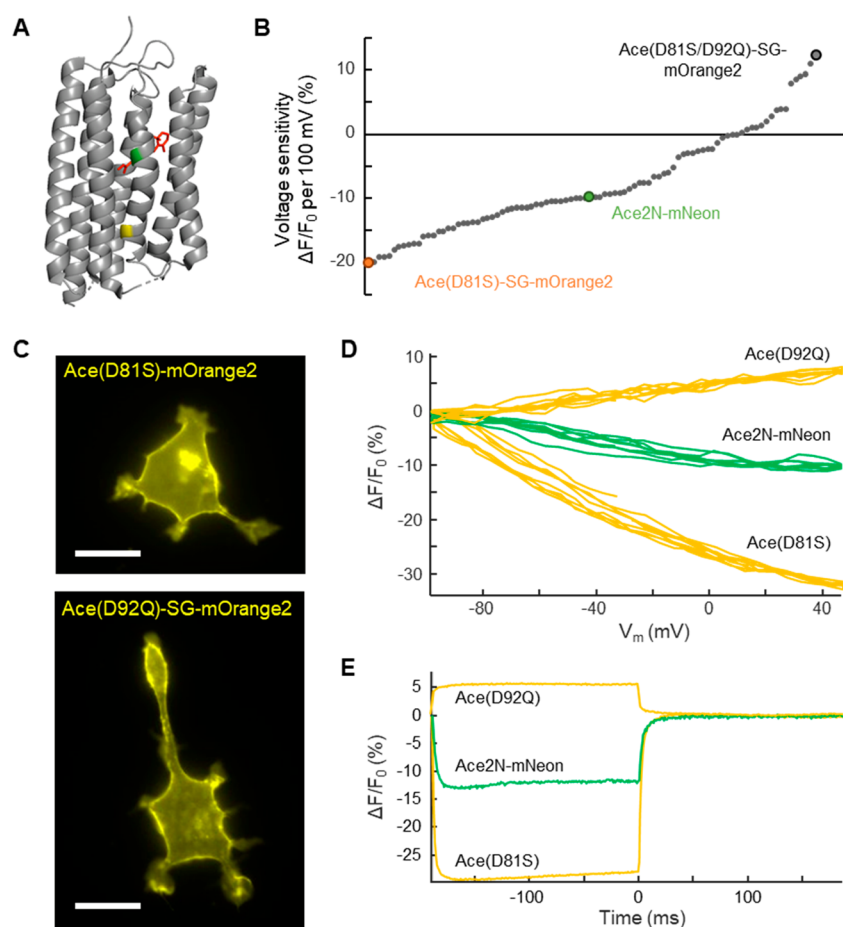


**Figure 1.** Screening of Ace mutants in HEK293T cells. (A) The Ace structure with Asp81 (green) and Asp92 (yellow) and the retinal (red). Asp81 and Asp92 act as proton acceptor and donor, respectively. The retinal chromophore is covalently linked to rhodopsin via the Schiff base. (B) Summary of voltage sensitivity of Ace-SG-mOrange2 mutants in HEK293T cells. (C) Wide-field epifluorescence image of HEK293T cell expressing Ace(D81S)-mOrange2 and Ace(D92Q)-SG-mOrange2. (D, E) Dynamic range and response kinetics of Ace2N-mNeon (green) and Ace mutant-mOrange2 fusion (yellow). To measure the dynamic range (D), membrane potential was varied linearly between  $-100$  and  $+50$  mV via whole-cell voltage clamp, and fluorescence images were acquired at a camera frame rate of 10 Hz. For kinetics measurements (E), membrane potential was altered from  $-70$  to  $+30$  mV and data were collected at a camera frame rate of 1058 Hz. Scale bar =  $20 \mu\text{m}$ .

**Table 1. Summary of eFRET GEVIs**

GEVI	fluorescence reporter (emission peak)	$-\Delta F/F_0$ per 100 mV (%) <sup>a</sup>	$-\Delta F/F_0$ per AP (%) <sup>b</sup>	SNR per AP <sup>b</sup>	<i>n</i>
Ace2N-mNeon	mNeonGreen (517 nm)	$10.0 \pm 0.2$	$5.2 \pm 0.3$	$18.2 \pm 4.2$	7
Ace(D81S)-mOrange2	mOrange2 (565 nm)	$25.9 \pm 1.0$	$9.1 \pm 0.3$	$40.2 \pm 8.6$	6
Ace(D81S)-mRuby4	mRuby4 (592 nm)	$9.1 \pm 0.4$	$3.6 \pm 0.3$	$18.7 \pm 3.6$	5
VARNAM	mRuby3 (592 nm)	$8.6 \pm 0.2$	$3.3 \pm 0.6$	$22.1 \pm 4.5$	5
Ace(D81S)-Halotag	TMR (574 nm)	$19.1 \pm 1.7$	$8.9 \pm 0.4$	$11.9 \pm 2.1$	6

<sup>a</sup>Measured in HEK293T cells. <sup>b</sup>Measured in cultured rat hippocampal neurons.

Another approach utilizes voltage-driven chemical equilibrium in microbial rhodopsins, which contain a retinal chromophore covalently linked to a lysine side chain via a Schiff base. Membrane potential modulates the acid–base equilibrium of the Schiff base, thus influencing the extinction coefficient of rhodopsin–retinal complex. QuasAr series employed the native retinal fluorescence as the reporter, which responds sensitively and rapidly to changes in the membrane potential, allowing faithful detection of APs both in vitro and in vivo.<sup>11–13</sup> However, both native and engineered rhodopsins<sup>13–16</sup> have low fluorescence quantum yields and require intense laser illumination with power densities ranging between  $80$  and  $300 \text{ W/cm}^2$ . To improve brightness, electrochromic FRET (eFRET) GEVIs were developed by

fusing rhodopsins with bright fluorescent proteins<sup>17–19</sup> or by conjugating with bright synthetic dyes.<sup>20,21</sup> These indicators exhibited good membrane trafficking, fast response kinetics, and high molecular brightness, yet they suffer from low voltage sensitivity. Recently, Pieribone et al. fused a red fluorescent protein, mRuby3, to a mutant Acetabulum (Ace) rhodopsin to achieve voltage imaging with relatively high sensitivity in the red spectrum.<sup>22</sup> However, mRuby3 exhibits relatively slow maturation or poor folding in living cells.

In this work, we independently describe the engineering of Ace rhodopsin to enhance its voltage sensitivity. Our efforts have resulted in two high-performance eFRET GEVIs: one with a significantly improved dynamic range, and one with a more red-shifted spectrum. Ace rhodopsin was first reported by

Boyden et al. in a screen to identify new light-driven proton pumps.<sup>23</sup> Through structure-guided mutagenesis and iterative rounds of screening, we successfully identified a mutant microbial rhodopsin fusion, Ace(D81S)-mOrange2, which exhibits good membrane trafficking, high photostability, and nearly 2-fold improvement in voltage sensitivity than the original Ace2N-mNeon sensor.<sup>19</sup> Notably, the same mutation has been independently identified by Pieribone et al.<sup>22</sup> We further red-shifted the emission spectrum by replacing mOrange2 with a newly developed bright and photostable red FP, mRuby4. Both FP-based GEVIs could be used jointly with optogenetic actuators to enable all-optical electrophysiology in cultured rat hippocampal neurons.

## RESULTS

### Screening of Ace Mutants with Improved Sensitivity in HEK293T Cells. We chose Ace rhodopsin as a starting

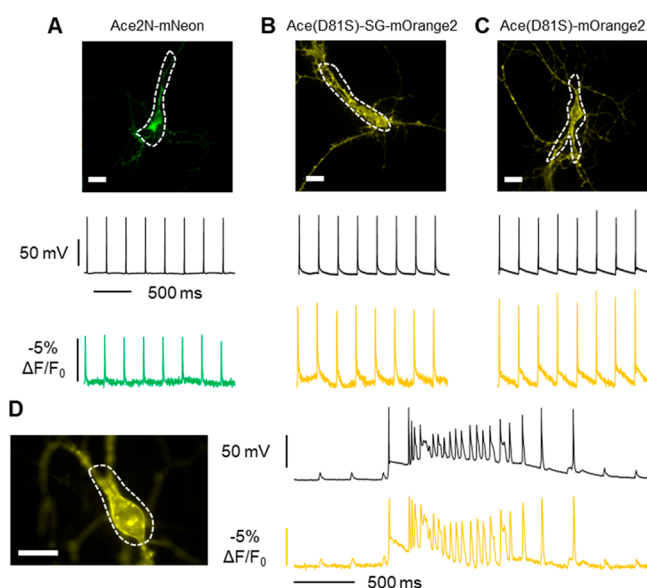


**Figure 2.** Voltage response of Ace(D81S)-mOrange2 in neuron cells. (A–C) Expression of Ace2N-mNeon (A), Ace(D81S)-SG-mOrange2 (B), and Ace(D81S)-mOrange2 (C) in cultured neurons, and their response to stimulated APs. (D) Voltage response of Ace(D81S)-mOrange2 to spontaneous APs in cultured rat hippocampus neurons. Images were acquired at a camera frame rate of 484 Hz. Scale bar = 20  $\mu\text{m}$ .

point for molecular evolution because it has better membrane trafficking and faster response kinetics than other rhodopsins when fused to FPs.<sup>19,20,24</sup> In addition, Ace could be paired with different colored fluorophores for eFRET voltage sensing due to its broad absorption spectrum. As shown in our previous work on eFRET indicators based on Ace and dyes, voltage sensitivity is highest when an orange fluorophore is fused to Ace.<sup>20</sup> We therefore chose mOrange2 as the FRET donor and fused it to the C-terminus of Ace via a short linker (Figure S1). To enhance FRET efficiency, we reduced the donor–acceptor distance by truncating 20 and 9 amino acid residues from the C-terminus of Ace and N-terminus of mOrange2, respectively, and inserted a Ser-Gly linker. This fusion, called Ace-SG-mOrange2, trafficked well to the plasma membrane in cultured human embryonic kidney 293T (HEK293T) cells and rat hippocampal neurons (Figure S1).

In Ace, Asp81 and Asp92 residues act as proton acceptor and proton donor, respectively, to the retinal<sup>25</sup> (Figure 1A). Because the voltage-sensing mechanism of Ace is closely related to the reversible protonation/deprotonation of the Schiff base, we reasoned that mutating either or both residues might lead to higher voltage sensitivity. We generated 127 Ace-SG-mOrange2 mutants and expressed them in HEK293T cells to screen more sensitive variants. Not surprisingly, some mutants showed poor expression and/or membrane trafficking (Figure S2) and were discarded for further analysis. For those that expressed well, we used whole-cell voltage clamp to change the membrane potential between  $-70$  mV to  $+30$  mV as square waves, while simultaneously monitoring mOrange2 fluorescence under a microscope. Voltage sensitivity was quantified as the ratio of fluorescence change over baseline fluorescence,  $\Delta F/F_0$  (per 100 mV depolarization, unless otherwise indicated), and response time constants were extracted from fitting the fluorescence trace to exponential decay functions. These voltage sensitivity results are summarized in Figure 1B.

Our small-scale screening revealed that both D81S and D81Y mutations could enhance the voltage sensitivity of Ace-SG-mOrange2 ( $-20\%$  and  $-17\%$  vs  $-12\%$   $\Delta F/F_0$ ) by 66% and 42%, respectively. Surprisingly, D81S retained millisecond time scale response ( $\tau = 2.1$  ms), while D81Y was 2.2 times slower ( $\tau = 4.7$  ms, Figure S3), indicating that position 81 in Ace affects voltage sensitivity and kinetics in different ways. D81S, like most other mutants, exhibited a negative slope in the fluorescence–voltage ( $F$ – $V$ ) response curve, as previous eFRET GEVIs. However, when Asp92 was mutated to noncharged residue Gln, the slope of its  $F$ – $V$  curve became positive ( $\sim 4.0\%$   $\Delta F/F_0$ , Figure 1C–E). Interestingly, D81S mutation could also improve the voltage sensitivity in these “positively-responding” mutants ( $\sim 11\%$   $\Delta F/F_0$ ), although response kinetics was slowed down to  $\tau \sim 30$  ms (Figure S4). Further mutations in residues surrounding the retinal chromophore did not generate any better mutants (Figure S5).

To improve the voltage response of Ace(D81S)-SG-mOrange2, we optimized the amino acid sequences between the rhodopsin and the fluorescent protein. Removing another four amino acid residues between Ace and mOrange2 (Figure S6) further improved voltage sensitivity by 25% while preserving good membrane trafficking in cells ( $-25.1 \pm 1.0\%$   $\Delta F/F_0$ ) (Figures 1C–E and S7, and Table 1). We called this linker-optimized fusion Ace(D81S)-mOrange2 and used it for subsequent experiments. Taken together, we have achieved a 2.5-fold improvement of sensitivity compared with the previously published Ace2N-mNeon ( $-10.0 \pm 0.2\%$   $\Delta F/F_0$ , Table 1).

**Detection of Neuronal Action Potentials with Ace-(D81S)-mOrange2/TMR.** The high sensitivity and fast response speed of Ace(D81S)-mOrange2 allowed for optical recording of action potential (AP) spike trains. We transfected cultured rat hippocampal neurons with Ace(D81S)-mOrange2 at DIV (days in vitro) 8–9, and observed good expression and membrane trafficking of the sensor after 4–5 days. We applied whole-cell patch clamp to stimulate AP firing, and simultaneously recorded electrical and optical signal under a fluorescence microscope. In terms of fractional fluorescence change,  $\Delta F/F_0$ , Ace(D81S)-mOrange2 achieved a sensitivity of  $-9.1 \pm 0.3\%$  in reporting AP spikes, which showed 75% improvement over Ace2N-mNeon ( $-5.2 \pm 0.3\%$  per AP) and no significant changes in the full-width at half maxima (fwhm)

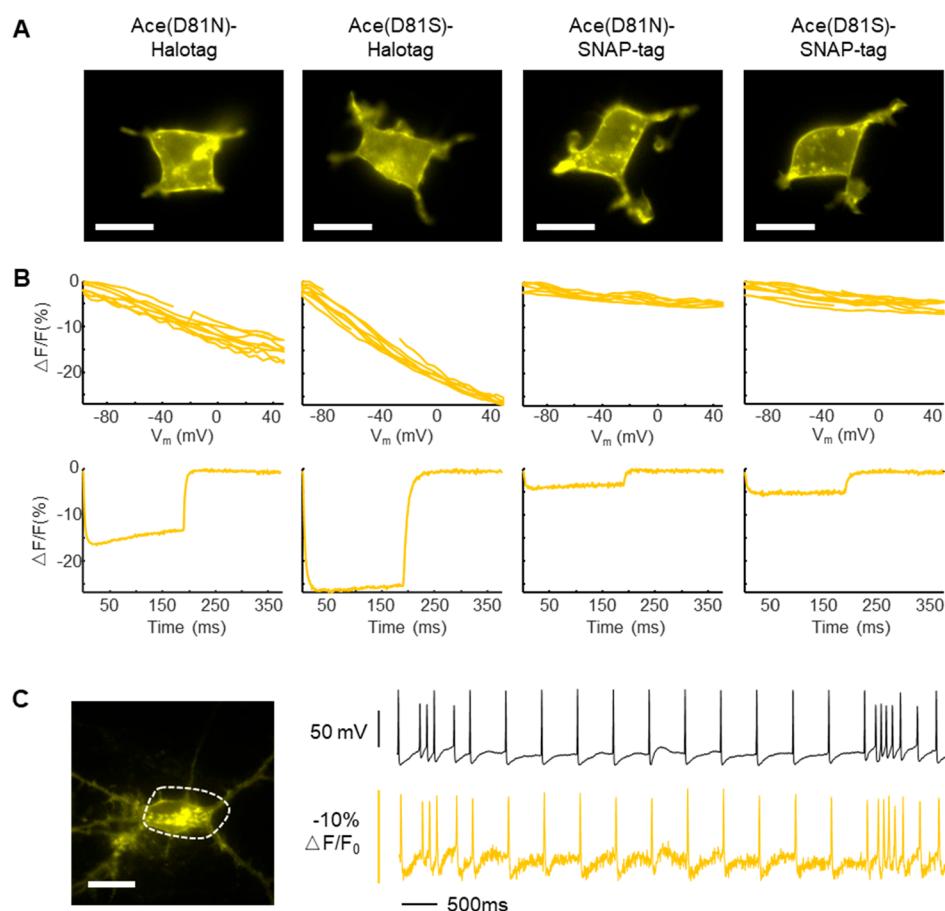


**Figure 3.** Characterization of hybrid GEVIs with Ace(D81S) mutation. (A) Fluorescence images of HEK293T cells expressing Ace(D81N/S)-Halotag (labeled with 5  $\mu$ M TMR-Halotag ligand) or Ace(D81N/S)-SNAP-tag (labeled with 3  $\mu$ M TMR-SNAP-tag ligand). (B) Dynamic range (upper panel) and response kinetics (lower panel) measured in whole-cell patch clamped HEK293T cells. (C) Fluorescence response of TMR-labeled Ace(D81S)-Halotag to APs in cultured neurons. Images were acquired at a camera frame rate of 484 Hz. Scale bar = 20  $\mu$ m.

of APs (Figures 2A–C and S8). The high signal-to-noise ratio (SNR) of Ace(D81S)-mOrange2 ( $40.2 \pm 8.6$  per AP) allowed for resolving spontaneous neuronal AP spike trains as well as detecting subthreshold voltage changes ( $\text{SNR} = 16.0 \pm 2.2$  per  $23 \pm 2$  mV) in cultured rat hippocampal neurons (Figure 2D).

Optical recording of neuronal activity could, in principle, complement electrode-based recording to map neuronal connectivity within a complex network. As a demonstration in cultured rat hippocampal neurons, we applied whole-cell current clamp to record membrane potential from one neuron and used Ace(D81S)-mOrange2 to monitor the AP activities in neighboring neurons. Neuronal activities between adjacent cells appeared synchronized (Figure S9), which could arise from either monosynaptic connection between the pair or synchronous network activity. The above examples demonstrated the feasibility of combining electrical-based stimulation and optical recording to dissect the neuronal functional connectivity network.

An advantage of eFRET is the modular design: the voltage-sensing rhodopsin scaffold could be in principle combined with various fluorescence reporters. While fluorescent proteins have been widely used as fluorescence reporters in sensor design, their photophysical properties, such as molecular brightness and photostability, are typically inferior to synthetic fluorophores. We sought to replace fluorescent protein with genetically encoded self-labeling tags, Halotag and SNAP-tag, which serve as anchors of synthetic dyes.<sup>20,21,26–28</sup> Both

protein tags can incorporate the red dye tetramethylrhodamine (TMR) efficiently<sup>29</sup> and could, in theory, efficiently transfer energy to Ace(D81S) due to large spectral overlap between the emission of TMR and the absorption of Ace(D81S).

We fused Halotag or SNAP-tag to the C-terminus of Ace(D81N) and Ace(D81S), respectively. To test voltage sensitivity, we expressed these fusion proteins in HEK293T cells and labeled them with TMR-halo ligand. Fluorescence images showed good membrane staining pattern (Figure 3A). We measured the voltage sensitivity using whole-cell patch clamp and fluorescence microscopy following the same protocol as described in the previous section. Ace(D81S)-Halotag had a linear  $F$ - $V$  response relationship from  $-100$  to  $50$  mV (Figures 3B and S10), with a sensitivity of  $-19.1 \pm 1.7\%$   $\Delta F/F_0$  per 100 mV membrane potential change (Figure 3B and Table 1), which is 1.6 times as sensitive as Ace(D81N)-Halotag ( $-11.7 \pm 0.7\%$   $\Delta F/F_0$ , also known as Voltron<sup>21</sup>). Consistent with previous observations in Ace2N-mNeon,<sup>19</sup> Ace(D81N)-Halotag exhibited a nonmonotonic, “peak” and “steady state” response to voltage steps. In contrast, the voltage response of Ace(D81S) can be better described as a double-exponential decay. This improved monotonicity in response curve could simplify data analysis when extracting voltage information from optical traces. Surprisingly, little voltage sensitivity was observed ( $<5\%$   $\Delta F/F_0$ ) for SNAP-tag fusions (Figure 3A, B), presumably due to low FRET efficiency. While Ace(D81S)-Halotag/TMR is slightly less

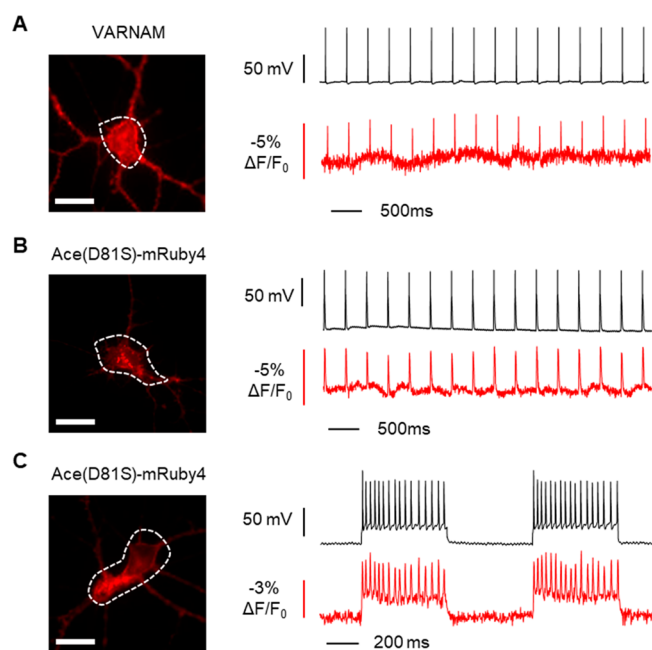


**Figure 4.** Voltage imaging of spontaneous and stimulated APs with Ace(D81S)-mRuby4 in cultured neurons. Left: Fluorescence images of rat hippocampal neurons expressing VARNAM (A) and Ace(D81S)-mRuby4 (B, C). Right: Voltage imaging of stimulated APs with VARNAM (A) and Ace(D81S)-mRuby4 (B, C). Images were acquired at a camera frame rate of 484 Hz. Scale bar = 20  $\mu\text{m}$ .

sensitive than Ace(D81S)-mOrange2 in HEK293T cells ( $-19.1 \pm 1.7\%$  vs  $-25.9 \pm 1.0\%$  per 100 mV), their performances in neurons are quite similar ( $-9.1 \pm 0.3\%$  vs  $-8.9 \pm 0.4\%$ ). The SNR is lower for Ace(D81S)-Halotag/TMR compared to Ace(D81S)-mOrange2 ( $11.9 \pm 2.1$  vs  $40.2 \pm 8.6$  per AP), due to lower brightness.

In cultured rat hippocampal neurons, Ace(D81S)-Halotag was capable of reporting stimulated APs with a sensitivity of  $-8.9 \pm 0.4\% \Delta F/F_0$  and SNR of  $11.9 \pm 2.1$  per AP (Figure 3C and Table 1). These data suggest that the sensitivity-enhancing

effect of D81S mutation identified from Ace-FP screening is transferable to hybrid sensor design.

**Development of a Bright and Photostable Red GEVI Based on Ace(D81S).** While the emission spectra of mOrange2 and TMR (emission peak  $\lambda_{\text{max}}$  at 565–574 nm) are red-shifted relative to the original green indicator Ace2N-mNeon ( $\lambda_{\text{max}}$  at 517 nm), they are still in the orange range. To further shift the emission spectrum into the red, we fused Ace(D81S) to a newly developed bright, monomeric, fast-maturing and photostable red FP, mRuby4 (see the Supporting Information). When this paper was under preparation, Pieribone et al. have independently discovered the D81S mutation that enhanced the voltage sensitivity of Ace-mRuby3 (VARNAM).<sup>22</sup> We measured the response kinetics and dynamic range of VARNAM and Ace(D81S)-mRuby4 in HEK293T cells (Figure S11), which revealed comparable voltage sensitivity ( $-8.6 \pm 0.2\%$  vs  $-9.1 \pm 0.4\% \Delta F/F_0$  per 100 mV, Table 1), that is both significantly lower than Ace(D81S)-mOrange2 ( $-25.9 \pm 1.0\%$ , Table 1). This spectral dependence of sensitivity is expected from the eFRET mechanism.<sup>17,20</sup>

We fused TS-ER2 localization sequences to the C terminus of mRuby4 to improve its membrane trafficking in cultured rat hippocampal neurons. Using cytosolic BFP or RFP as a marker for cell morphology, we compared the trafficking of GEVIs listed in Table 1. As shown in Figures S12–S17, the membrane targeting of both Ace(D81S)-mRuby4 and VARNAM appears worse than Ace(D81S)-mOrange2 across five randomly selected fields of view. Both Ace(D81S)-mRuby4 and VARNAM are capable of reporting stimulated action potentials with comparable sensitivity in cultured rat hippocampal neurons ( $-3.6 \pm 0.3\%$  vs  $-3.3 \pm 0.6\% \Delta F/F_0$  per AP, Figure 4 and Table S1). In terms of photostability, the half-life of Ace(D81S)-mRuby4 is 25% longer than Ace(D81S)-mRuby3 (VARNAM) in cultured neurons under continuous 561 nm laser illumination ( $t_{1/2} = 475 \pm 23$  s vs  $381 \pm 9$  s, mean  $\pm$  SEM).

Unlike Ace2N-mNeon, which spectrally overlaps with optogenetic actuators such as channelrhodopsin, the red-shifted spectrum of Ace(D81S)-mOrange2/mRuby4 could

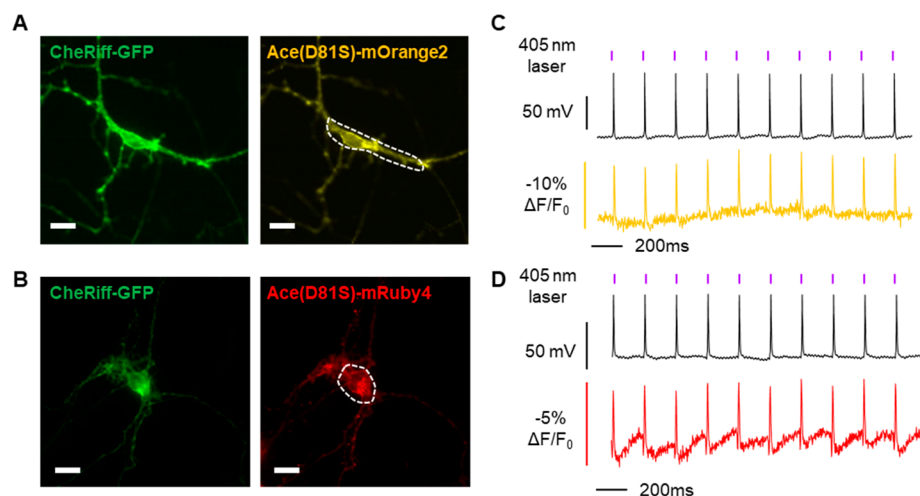


**Figure 5.** All-optical electrophysiology with Ace(D81S)-mOrange2/mRuby4. (A, B) Fluorescence images showing coexpression of CheRiff channelrhodopsin with either Ace(D81S)-mOrange2 (A) or Ace(D81S)-mRuby4 (B) in cultured rat hippocampus neurons. (C, D) Voltage imaging of AP firing in mOrange2 (C) or mRuby4 (D) channels, when neurons were optogenetically stimulated by a pulsed purple laser (405 nm). Images were acquired at a camera frame rate of 484 Hz. Scale bar = 20  $\mu\text{m}$ .

enable all-optical stimulation and recording of neuronal activities. We coexpressed CheRiff channelrhodopsin<sup>13</sup> and Ace(D81S)-mOrange2/mRuby4 in cultured rat hippocampal neurons (Figure 5A, B), and applied 405 and 561 nm lasers to activate CheRiff and to excite mOrange2/mRuby4, respectively. Robust firing of APs upon pulsed 405 nm light illumination was detected by fluorescence imaging of mOrange2 (Figure 5C) or mRuby4 (Figure 5D). We noted that the fluorescence trace of Ace(D81S)-mRuby4 deviated from the voltage trace during CheRiff-evoked AP. This phenomenon was not observed when neurons were stimulated via whole-cell current clamp (Figure 4), and this was not due to photochromic behavior (Figure S18). This anomaly suggests that, at least in all-optical electrophysiology measurements described above, Ace(D81S)-mRuby4 is better at giving accurate spiking timing information than revealing the detailed AP waveform information.

## DISCUSSION

Red-shifted GEVIs have several advantages over GFP-based ones, such as multiplexed imaging and better tissue penetration.<sup>2</sup> In this study, we have developed a panel of red-shifted eFRET GEVIs based on an Ace rhodopsin mutant carrying a single mutation, D81S, which dramatically improved its sensitivity toward membrane potential. When paired with Ace(D81S), mOrange2 and mRuby4 exhibit the largest dynamic range and the reddest spectrum, respectively, among all eFRET GEVIs, enabling all-optical electrophysiology in cultured neurons. We further demonstrated that the same mutation could be employed to enhance the voltage sensitivity of hybrid voltage indicator Ace-Halotag, thus highlighting the feature of modular design in eFRET indicators.

Our results revealed that Asp81 and Asp92 residues critically influenced the dynamic range, kinetics and response polarity of the rhodopsin. This observation is consistent with their roles as proton acceptor and donor in the native proton pumping pathway of wild-type Ace and the eFRET voltage-sensing mechanism. While both aspartic acid residues appear highly conserved among rhodopsins, naturally occurring serine or threonine mutations have been observed in the halorhodopsin<sup>30</sup> and GtACR1<sup>31</sup> rhodopsins (Figure S19). Our screening also identified D92Q mutation that reversed the polarity of the  $F-V$  response, which, to the best of our knowledge, is the first example of positively responding eFRET GEVI and may serve as a starting point of future engineering.

As we prepared this paper, a red GEVI based on Ace(D81S) and mRuby3 was published.<sup>22</sup> This indicator, called VARNAM, is capable of reporting synaptic potentials in both acute brain slice and in vivo. Compared to mRuby3, our new red FP mRuby4 is brighter, has higher photostability, and matures more completely, thus making it an attractive choice for future in vivo long-term imaging experiments. In cultured neurons, our Ace(D81S)-mOrange2 indicator exhibited higher sensitivity than VARNAM. While all these red-shifted GEVIs worked well in cultured neurons, three questions need to be addressed: (1) We have yet to compare their performance in slices or in vivo. (2) All GEVIs tested in this study showed some intracellular puncta when expressed in neurons, indicating incomplete membrane trafficking. This is detrimental to the signal-to-noise ratio and needs to be addressed in future engineering. (3) Previous studies have shown that the response amplitude of rhodopsin-based GEVIs is often

dramatically reduced under two-photon illumination,<sup>10,32</sup> which could limit their applications in vivo.

Our newly developed red-shifted GEVIs still have a low dynamic range compared to the state-of-the-art calcium sensors. Future studies on voltage sensitivity improvement of eFRET GEVIs could be focused on three directions: First, large-scale high-throughput screening could be performed on Ace(D81S) by adopting automatic cell-based screening platform. Second, engineering of brighter orange/red FPs could be achieved by improving existing orange FPs, such as mOrange2 and mKO $\kappa$ ,<sup>33</sup> or blue shifting red or far-red FPs, such as the mNeptune family.<sup>34</sup> Third, our recently developed hybrid indicator Flare1 achieved high sensitivity ( $\Delta F/F_0 = -35.9\%$  per 100 mV) via direct fluorophore conjugation with Ace.<sup>20</sup> This might be further improved by introducing Ace mutations identified in this study.

## METHODS

See the Supporting Information.

## ASSOCIATED CONTENT

### Supporting Information

The Supporting Information is available free of charge at <https://pubs.acs.org/doi/10.1021/acschemneuro.9b00501>.

Molecular cloning; fluorescence microscopy; voltage imaging and electrophysiology; Halotag labeling; mRuby4 engineering; full sequences of genetic constructs used in the study (PDF)

## AUTHOR INFORMATION

### Corresponding Authors

\*E-mail: [jun.chu@siat.ac.cn](mailto:jun.chu@siat.ac.cn) (J.C.).

\*E-mail: [zoupeng@pku.edu.cn](mailto:zoupeng@pku.edu.cn) (P.Z.).

### ORCID

Peng Zou: 0000-0002-9798-5242

### Present Address

#S.Z.: Department of Minimally Invasive Intervention, Peking University Shenzhen Hospital, Shenzhen 518036, China.

### Author Contributions

Y.X., M.D., S.Z., and J.Y. contributed equally to this work. Y.X., J.C. and P.Z. conceived and designed the experiments. Y.X. performed sensitivity screening in HEK293T cells and voltage imaging in neurons. J.Y. designed and tested hybrid GEVI. M.D. and S.Z. performed protein mutagenesis and characterization of mRuby4. L.P. developed data analysis software. Y.X., M.D., J.Y., J.C. and P.Z. wrote the paper.

### Funding

This work was supported by National Key Research and Development Program of China (2017YFA0700403), National Natural Science Foundation of China (Grant 21673009, 21727806, 91753131, 31670872, 21874145), Shenzhen Science and Technology Innovation Committee (Grant KQJSCX20170331161420421, JCYJ20170818163925063, JCYJ20170818164040422), and Peking-Tsinghua Center for Life Sciences. P.Z. was supported by the National Thousand Young Talents Award. J.C. was supported by the "Hundred Talents" Program award from the Chinese Academy of Sciences. M.D. was supported by China Postdoctoral Science Foundation (Grant 2018M633180).

### Notes

The authors declare no competing financial interest.

## REFERENCES

- (1) Miller, E. W. (2016) Small molecule fluorescent voltage indicators for studying membrane potential. *Curr. Opin. Chem. Biol.* 33, 74–80.
- (2) Xu, Y., Zou, P., and Cohen, A. E. (2017) Voltage imaging with genetically encoded indicators. *Curr. Opin. Chem. Biol.* 39, 1–10.
- (3) Wang, A., Feng, J., Li, Y., and Zou, P. (2018) Beyond Fluorescent Proteins: Hybrid and Bioluminescent Indicators for Imaging Neural Activities. *ACS Chem. Neurosci.* 9 (4), 639–650.
- (4) Dimitrov, D., He, Y., Mutoh, H., Baker, B. J., Cohen, L., Akemann, W., and Knopfel, T. (2007) Engineering and characterization of an enhanced fluorescent protein voltage sensor. *PLoS One* 2 (5), No. e440.
- (5) Jin, L., Han, Z., Platisa, J., Woollorton, J. R., Cohen, L. B., and Pieribone, V. A. (2012) Single action potentials and subthreshold electrical events imaged in neurons with a fluorescent protein voltage probe. *Neuron* 75 (5), 779–85.
- (6) Abdelfattah, A. S., Farhi, S. L., Zhao, Y., Brinks, D., Zou, P., Ruangkittsakul, A., Platisa, J., Pieribone, V. A., Ballanyi, K., Cohen, A. E., and Campbell, R. E. (2016) A Bright and Fast Red Fluorescent Protein Voltage Indicator That Reports Neuronal Activity in Organotypic Brain Slices. *J. Neurosci.* 36 (8), 2458–72.
- (7) St-Pierre, F., Marshall, J. D., Yang, Y., Gong, Y., Schnitzer, M. J., and Lin, M. Z. (2014) High-fidelity optical reporting of neuronal electrical activity with an ultrafast fluorescent voltage sensor. *Nat. Neurosci.* 17 (6), 884–9.
- (8) Akemann, W., Mutoh, H., Perron, A., Park, Y. K., Iwamoto, Y., and Knopfel, T. (2012) Imaging neural circuit dynamics with a voltage-sensitive fluorescent protein. *J. Neurophysiol.* 108 (8), 2323–37.
- (9) Yang, H. H., St-Pierre, F., Sun, X., Ding, X., Lin, M. Z., and Clandinin, T. R. (2016) Subcellular Imaging of Voltage and Calcium Signals Reveals Neural Processing In Vivo. *Cell* 166 (1), 245–57.
- (10) Chamberland, S., Yang, H. H., Pan, M. M., Evans, S. W., Guan, S., Chavarha, M., Yang, Y., Salesse, C., Wu, H., Wu, J. C., Clandinin, T. R., Toth, K., Lin, M. Z., and St-Pierre, F. (2017) Fast two-photon imaging of subcellular voltage dynamics in neuronal tissue with genetically encoded indicators. *eLife* 6, e25690.
- (11) Kralj, J. M., Hochbaum, D. R., Douglass, A. D., and Cohen, A. E. (2011) Electrical spiking in *Escherichia coli* probed with a fluorescent voltage-indicating protein. *Science* 333 (6040), 345–8.
- (12) Kralj, J. M., Douglass, A. D., Hochbaum, D. R., Maclaurin, D., and Cohen, A. E. (2012) Optical recording of action potentials in mammalian neurons using a microbial rhodopsin. *Nat. Methods* 9 (1), 90–5.
- (13) Hochbaum, D. R., Zhao, Y., Farhi, S. L., Klapoetke, N., Werley, C. A., Kapoor, V., Zou, P., Kralj, J. M., Maclaurin, D., Smedemark-Margulies, N., Saulnier, J. L., Boulting, G. L., Straub, C., Cho, Y. K., Melkonian, M., Wong, G. K., Harrison, D. J., Murthy, V. N., Sabatini, B. L., Boyden, E. S., Campbell, R. E., and Cohen, A. E. (2014) All-optical electrophysiology in mammalian neurons using engineered microbial rhodopsins. *Nat. Methods* 11 (8), 825–33.
- (14) Piatkevich, K. D., Jung, E. E., Straub, C., Linghu, C., Park, D., Suk, H. J., Hochbaum, D. R., Goodwin, D., Pnevmatikakis, E., Pak, N., Kawashima, T., Yang, C. T., Rhoades, J. L., Shemesh, O., Asano, S., Yoon, Y. G., Freifeld, L., Saulnier, J. L., Riegler, C., Engert, F., Hughes, T., Drobizhev, M., Szabo, B., Ahrens, M. B., Flavell, S. W., Sabatini, B. L., and Boyden, E. S. (2018) A robotic multidimensional directed evolution approach applied to fluorescent voltage reporters. *Nat. Chem. Biol.* 14 (4), 352–360.
- (15) McIsaac, R. S., Engqvist, M. K., Wannier, T., Rosenthal, A. Z., Herwig, L., Flytzanis, N. C., Imasheva, E. S., Lanyi, J. K., Balashov, S. P., Gradinaru, V., and Arnold, F. H. (2014) Directed evolution of a far-red fluorescent rhodopsin. *Proc. Natl. Acad. Sci. U. S. A.* 111 (36), 13034–9.
- (16) Flytzanis, N. C., Bedbrook, C. N., Chiu, H., Engqvist, M. K., Xiao, C., Chan, K. Y., Sternberg, P. W., Arnold, F. H., and Gradinaru, V. (2014) Archaelhodopsin variants with enhanced voltage-sensitive fluorescence in mammalian and *Caenorhabditis elegans* neurons. *Nat. Commun.* 5, 4894.
- (17) Zou, P., Zhao, Y., Douglass, A. D., Hochbaum, D. R., Brinks, D., Werley, C. A., Harrison, D. J., Campbell, R. E., and Cohen, A. E. (2014) Bright and fast multicoloured voltage reporters via electrochromic FRET. *Nat. Commun.* 5, 4625.
- (18) Gong, Y., Wagner, M. J., Zhong Li, J., and Schnitzer, M. J. (2014) Imaging neural spiking in brain tissue using FRET-opsin protein voltage sensors. *Nat. Commun.* 5, 3674.
- (19) Gong, Y., Huang, C., Li, J. Z., Grewe, B. F., Zhang, Y., Eismann, S., and Schnitzer, M. J. (2015) High-speed recording of neural spikes in awake mice and flies with a fluorescent voltage sensor. *Science* 350 (6266), 1361–6.
- (20) Xu, Y., Peng, L., Wang, S., Wang, A., Ma, R., Zhou, Y., Yang, J., Sun, D. E., Lin, W., Chen, X., and Zou, P. (2018) Hybrid Indicators for Fast and Sensitive Voltage Imaging. *Angew. Chem., Int. Ed.* 57 (15), 3949–3953.
- (21) Abdelfattah, A. S., Kawashima, T., Singh, A., Novak, O., Liu, H., Shuai, Y., Huang, Y.-C., Grimm, J. B., Patel, R., Friedrich, J., Mensh, B. D., Paninski, L., Macklin, J. J., Podgorski, K., Lin, B.-J., Chen, T.-W., Turner, G.-C., Liu, Z., Koyama, M., Svoboda, K., Ahrens, M. B., Lavis, L. D., and Schreite, E. R. (2019) Bright and photostable chemigenetic indicators for extended *in vivo* voltage imaging. *Science* 365, 699.
- (22) Kannan, M., Vasani, G., Huang, C., Haziza, S., Li, J. Z., Inan, H., Schnitzer, M. J., and Pieribone, V. A. (2018) Fast, *in vivo* voltage imaging using a red fluorescent indicator. *Nat. Methods* 15 (12), 1108–1116.
- (23) Chow, B. Y., Han, X., Dobry, A. S., Qian, X., Chuong, A. S., Li, M., Henninger, M. A., Belfort, G. M., Lin, Y., Monahan, P. E., and Boyden, E. S. (2010) High-performance genetically targetable optical neural silencing by light-driven proton pumps. *Nature* 463 (7277), 98–102.
- (24) Tsunoda, S. P., Ewers, D., Gazzarrini, S., Moroni, A., Gradmann, D., and Hegemann, P. (2006) H<sup>+</sup>-pumping rhodopsin from the marine alga *Acetabularia*. *Biophys. J.* 91 (4), 1471–9.
- (25) Wada, T., Shimono, K., Kikukawa, T., Hato, M., Shinya, N., Kim, S. Y., Kimura-Someya, T., Shirouzu, M., Tamogami, J., Miyauchi, S., Jung, K. H., Kamo, N., and Yokoyama, S. (2011) Crystal structure of the eukaryotic light-driven proton-pumping rhodopsin, *Acetabularia* rhodopsin II, from marine alga. *J. Mol. Biol.* 411 (5), 986–98.
- (26) Brun, M. A., Griss, R., Reymond, L., Tan, K. T., Piguet, J., Peters, R. J., Vogel, H., and Johnsson, K. (2011) Semisynthesis of fluorescent metabolite sensors on cell surfaces. *J. Am. Chem. Soc.* 133 (40), 16235–42.
- (27) Masharina, A., Reymond, L., Maurel, D., Umezawa, K., and Johnsson, K. (2012) A fluorescent sensor for GABA and synthetic GABA(B) receptor ligands. *J. Am. Chem. Soc.* 134 (46), 19026–34.
- (28) Brun, M. A., Tan, K. T., Griss, R., Kielkowska, A., Reymond, L., and Johnsson, K. (2012) A semisynthetic fluorescent sensor protein for glutamate. *J. Am. Chem. Soc.* 134 (18), 7676–8.
- (29) Liss, V., Barlag, B., Nietschke, M., and Hensel, M. (2016) Self-labelling enzymes as universal tags for fluorescence microscopy, super-resolution microscopy and electron microscopy. *Sci. Rep.* 5, 17740.
- (30) Engelhard, C., Chizhov, I., Siebert, F., and Engelhard, M. (2018) Microbial Halorhodopsins: Light-Driven Chloride Pumps. *Chem. Rev.* 118 (21), 10629–10645.
- (31) Kato, H. E., Kim, Y. S., Paggi, J. M., Evans, K. E., Allen, W. E., Richardson, C., Inoue, K., Ito, S., Ramakrishnan, C., Fenno, L. E., Yamashita, K., Hilger, D., Lee, S. Y., Berndt, A., Shen, K., Kandori, H., Dror, R. O., Kobilka, B. K., and Deisseroth, K. (2018) Structural mechanisms of selectivity and gating in anion channelrhodopsins. *Nature* 561 (7723), 349–354.
- (32) Brinks, D., Klein, A. J., and Cohen, A. E. (2015) Two-Photon Lifetime Imaging of Voltage Indicating Proteins as a Probe of Absolute Membrane Voltage. *Biophys. J.* 109 (5), 914–21.
- (33) Tsutsui, H., Karasawa, S., Okamura, Y., and Miyawaki, A. (2008) Improving membrane voltage measurements using FRET with new fluorescent proteins. *Nat. Methods* 5 (8), 683–5.

(34) Chu, J., Haynes, R. D., Corbel, S. Y., Li, P., Gonzalez-Gonzalez, E., Burg, J. S., Ataie, N. J., Lam, A. J., Cranfill, P. J., Baird, M. A., Davidson, M. W., Ng, H. L., Garcia, K. C., Contag, C. H., Shen, K., Blau, H. M., and Lin, M. Z. (2014) Non-invasive intravital imaging of cellular differentiation with a bright red-excitable fluorescent protein. *Nat. Methods* 11 (5), 572–8.